

Mechanobiology of soft skeletal tissue differentiation— a computational approach of a fiber-reinforced poroelastic model based on homogeneous and isotropic simplifications

E. G. Lobo, T. A. L. Wren, G. S. Beaupré, D. R. Carter

83

Abstract The material properties of multipotent mesenchymal tissue change dramatically during the differentiation process associated with skeletal regeneration. Using a mechanobiological tissue differentiation concept, and homogeneous and isotropic simplifications of a fiber-reinforced poroelastic model of soft skeletal tissues, we have developed a mathematical approach for describing time-dependent material property changes during the formation of cartilage, fibrocartilage, and fibrous tissue under various loading histories. In this approach, intermittently imposed fluid pressure and tensile strain regulate proteoglycan synthesis and collagen fibrillogenesis, assembly, cross-linking, and alignment to cause changes in tissue permeability (k), compressive aggregate modulus (H_A), and tensile elastic modulus (E). In our isotropic model, k represents the permeability in the least permeable direction (perpendicular to the fibers) and E represents the tensile elastic modulus in the stiffest direction (parallel to the fibers). Cyclic fluid pressure causes an increase in proteoglycan synthesis, resulting in a decrease in k and increase in H_A caused by the hydrophilic nature and large size of the aggregating proteoglycans. It further causes a slight increase in E owing to the stiffness added by newly synthesized type II collagen. Tensile strain increases the density, size, alignment, and cross-linking of collagen fibers thereby increasing E while also decreasing k as a result of an increased flow path length. The Poisson's ratio of the solid matrix, ν_s , is assumed to remain constant (near zero) for all soft tissues. Implementing a computer algorithm based on these concepts, we simulate progressive changes in material properties for differentiating tissues. Beginning with initial values of $E=0.05$ MPa, $H_A=0$ MPa, and $k=1\times 10^{-13}$ m⁴/Ns for multipotent mesenchymal tissue, we predict final values of $E=11$ MPa, $H_A=1$ MPa, and $k=4.8\times 10^{-15}$ m⁴/Ns for articular cartilage, $E=339$ MPa, $H_A=1$ MPa, and $k=9.5\times 10^{-16}$ m⁴/Ns for fibrocartilage, and $E=1,000$ MPa, $H_A=0$ MPa, and $k=7.5\times 10^{-16}$ m⁴/Ns for fibrous tissue. These final values are consistent with the values reported by other investigators and the time-dependent acquisition of these values is consistent with current knowledge of the differentiation process.

1

Introduction and background

During skeletal development and regeneration multipotent mesenchymal tissue can differentiate into a variety of skeletal tissues including bone, cartilage, fibrocartilage, and fibrous tissue. The type of tissue that is formed depends on the cells available, the chemical environment, and the imposed mechanical stimuli. In a regenerating skeletal site that favors osteogenesis, intramembranous bone will form

Received: 28 November 2001 / Accepted: 29 April 2003

Published online: 17 July 2003

E. G. Lobo (✉), T. A. L. Wren, G. S. Beaupré, D. R. Carter
Biomechanical Engineering Division,
Mechanical Engineering Department,
Stanford University, Stanford, CA, 94305, USA
E-mail: eglobo@stanfordalumni.org
Tel.: +1-650-8144418
Fax: +1-650-7251587

E. G. Lobo, T. A. L. Wren, G. S. Beaupré, D. R. Carter
Rehabilitation R&D Center, VA Palo Alto Health Care System,
3801 Miranda Avenue/153, Palo Alto, CA 94304-1200, USA

We would like to thank Jay Henderson, Sandra Shefelbine, and Dr. R. Lane Smith for their helpful suggestions. Support for this work was provided by VA Merit Review project A501-4RA.

directly from the early multipotent mesenchymal tissue at the site, provided that the locally imposed cyclic mechanical forces are small. If significant compressive or tensile forces are present, however, cartilage, fibrocartilage, or fibrous tissue will be formed (Carter and Beaupré 2001). Using idealized, single phase constitutive models, previous investigators in our laboratory have proposed a semi-quantitative tissue differentiation concept relating cyclic hydrostatic stress and tensile strain to the formation of bone, cartilage, fibrous tissue, and fibrocartilage (Carter and Giori 1991; Giori et al. 1995; Carter et al. 1998; Carter and Beaupré 2001). We proposed that cartilage forms under excessive hydrostatic compressive stress, fibrous tissue forms with excessive tensile strain, and fibrocartilage forms with combined hydrostatic pressure in the presence of tensile strain. These ideas are consistent with the views of Pauwels (1980) and Claes and Heigele (1999).

We now expand these concepts to incorporate a constitutive model based on a fiber-reinforced, poroelastic representation of soft tissue (Li et al. 1999; Li et al. 2000) to describe the time-dependent differentiation of multipotent mesenchymal tissue. The controlling mechanical parameters are the imposed intermittent tensile strain and the locally generated cyclic fluid pressure (Fig. 1). Using this new constitutive model with an extended tissue differentiation concept, we create a computational model to describe the time-dependent changes in material properties of differentiating soft skeletal tissues in homogeneous strain states (Table 1, Fig. 2). The time-dependent material property changes are coupled conceptually to representations of the compositional changes in proteoglycans and collagen in the tissues. We do not attempt to model time-dependent changes associated with intramembranous bone formation. Our attention here is directed only at those loading histories that would lead to the formation of soft skeletal tissues, i.e., cartilage, fibrous tissue, and fibrocartilage.

Previous computational analyses of tissue differentiation have modeled tissue as either a linearly elastic, single phase (Carter et al. 1998; Carter et al. 2000; Claes and Heigele 1999; Meroi and Natali

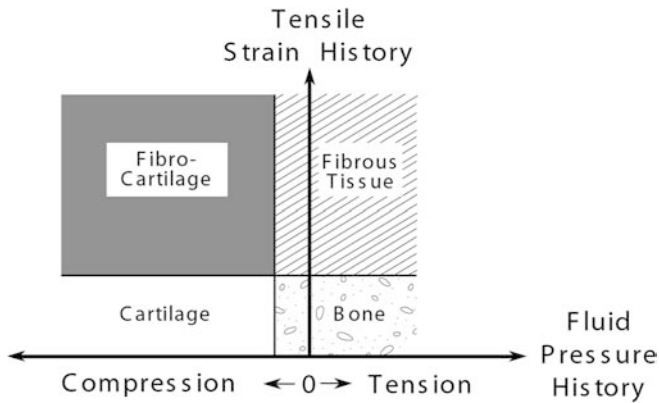


Fig. 1. Semi-quantitative tissue differentiation theory relating mechanical loading history to tissue phenotype. Mechanical loading history can be defined in terms of solid matrix tensile strains and fluid pressures in a fiber-reinforced poroelastic model. “Tension” on x axis corresponds to negative fluid pressure

Table 1. Mechanobiological effects of cyclic tensile strain and fluid pressure on material properties of differentiating tissue (tensile elastic modulus E , permeability k , and aggregate modulus H_A)

Mechanical stimulus	Physical mechanism	Physical effect	Effect on material properties	Reference
Cyclic tensile strain ϵ	Collagen I synthesis, assembly, cross-linking, alignment	Increased number, density, size, stiffness, cross-linking, alignment of type I collagen fibers	E increases via \dot{E}_ϵ	Fig. 3a; Eq. 4
		Increased flow path length caused by increased fiber size and packing density	k decreases via q_E	Fig. 5; Eq. 8
Cyclic fluid pressure p	Collagen II synthesis	Increased matrix stiffness caused by increased collagen content	E increases via $E_{f,p}$	Fig. 3b; Eqs. 5 and 6
		Increased flow path length caused by increased collagen content	k decreases via q_E	Fig. 5; Eq. 8
	Proteoglycan synthesis	Increased binding of water and packing of aggregates	k decreases via \dot{k}_p H_A increases	Fig. 4; Eq. 7 Fig. 3c
		Increased flow path length caused by increased size and denser packing of aggregates	E increases via H_A k decreases via q_E	Eqs. 5 and 6 Fig. 5; Eq. 8

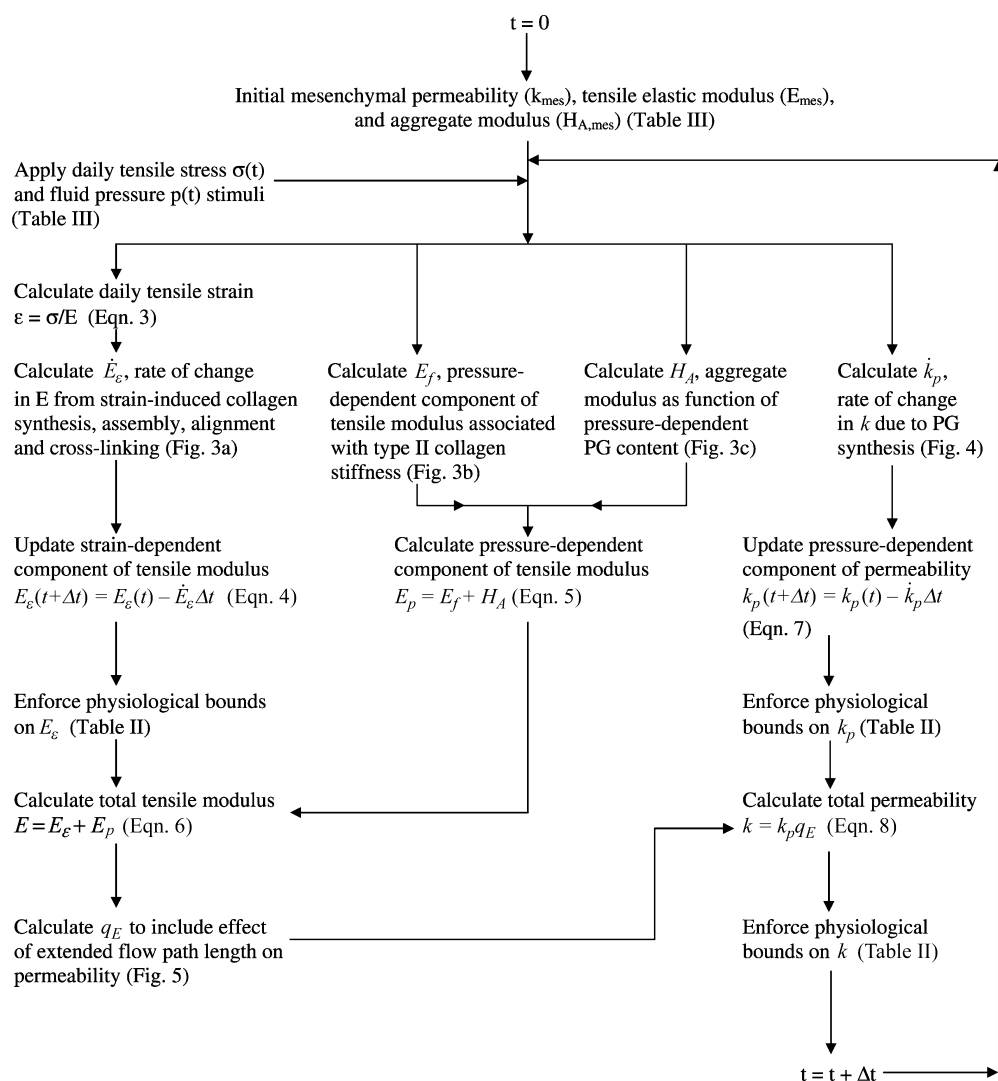


Fig. 2. Flowchart describing tissue differentiation algorithm used in the simulations

1989) or linear biphasic (Huijkes et al. 1997; Prendergast et al. 1997; Wren et al. 2000) material. Although linear elastic models can approximate biphasic models at short time intervals ($t=0+$) (Brown and Singerman 1986; Higgison and Snaith 1979) at slow loading rates a poroelastic or biphasic model may be more appropriate.

Poroelastic models are based on the consolidation theory developed by Biot to describe soil settlement under load through the process of “squeezing water out of an elastic porous medium” (Biot 1941). Biot’s initial theory assumed material isotropy. Later refinements included anisotropic and transversely isotropic materials (Biot 1955). These theories have been implemented as poroelastic constitutive models of soft skeletal tissues (Atkinson et al. 1997; Li et al. 1999; Wren et al. 2000).

Biphasic models based on the linear KLM theory (Mow et al. 1980) are also commonly used to model cartilage and other soft skeletal tissues (Joshi et al. 1995; Mow et al. 1980; Prendergast et al. 1997; Soltz and Ateshian 1998). The mathematical implementation and solution of the linear biphasic approach are identical to that of the poroelastic approach when incompressibility is assumed (Levenston et al. 1998). A linear poroelastic or biphasic material model can be characterized by three material properties: the compressive aggregate modulus (H_A), the Poisson’s ratio of the drained solid matrix (ν_s), and the permeability (k). As is common in linear poroelastic models, the fluid phase is assumed to be incompressible with a Poisson’s ratio equal to 0.5. Experiments have been conducted to determine the values for these parameters in cartilage (Ateshian et al. 1997; Brown and Singerman 1986; Soltz and Ateshian 2000), fibrocartilage (Haridas et al. 1998; Joshi et al. 1995), and fibrous tissue (Haridas et al. 1998; Weiss et al. 2000). Experimental values have not yet been determined for differentiating multipotent mesenchymal tissue.

As multipotent mesenchymal tissue differentiates, it experiences changes in both its tensile and compressive properties. In this study, we track material property adaptations of mesenchymal tissue as it differentiates into both fibrous and chondroid tissue and are therefore interested in both tensile and compressive properties. To accomplish this, we implement a fiber-reinforced poroelastic model of mesenchymal tissue that incorporates the effects of collagen fiber reinforcement in a fluid-saturated, proteoglycan solid matrix. Our approach is based on recent analyses by other investigators who have modeled cartilage using fibril reinforced poroelastic (Li et al. 1999; Li et al. 2000) and fibril reinforced biphasic (Soulhat et al. 1999) models. Such fibril reinforced biphasic and poroelastic models of articular cartilage attempt to capture experimentally observed tension-compression nonlinearities in cartilage, a behavior that has been difficult to describe using a biphasic model alone (Li et al. 1999). These constitutive models are described using four material properties: tensile elastic modulus (E), compressive aggregate modulus (H_A), permeability (k), and the solid matrix Poisson's ratio (ν_s). In this study, we simulate time-dependent changes in three of these material properties during mesenchymal tissue differentiation using an isotropic model: E , H_A , and k . The values of ν_s derived from biphasic analyses of indentation experiments in cartilage are close to zero (Athanasίου et al. 1991; Jurvelin et al. 1997; Mow et al. 1989; Mow et al. 1991). We expect similar behavior for multipotent mesenchymal tissue and assume that the value of ν_s is constant and equal to zero for all soft tissues under consideration here.

It has been shown that both proteoglycan (Gu et al. 1999; Roughley and Lee 1994) and collagen fiber content (Chen et al. 1998; Weiss et al. 2000) affect the permeability of a tissue. Proteoglycan aggregates, because of their large size and hydrophilic nature, decrease k (Mansour and Mow 1976). Increased collagen fiber content further decreases k through increased fiber size and density resulting in an extended flow path length for fluid to traverse (Chen et al. 1998; Weiss et al. 2000). The collagen fiber content also affects E with increases in fiber content, size, cross-linking, and alignment resulting in corresponding increases in E (Wren et al. 1998; Wren and Carter 1998).

Changes in collagen and proteoglycan content can occur in response to mechanical loading. Previous investigators have found that type I collagen fibrillogenesis is up-regulated by fibroblasts exposed to cyclic tensile strain (Howard et al. 1998). This leads to a corresponding increase in fiber size with fiber alignment along the direction of tensile strain (Ilizarov 1989). Other investigators have found that both proteoglycan and type II collagen synthesis are up-regulated by chondrocytes exposed to cyclic hydrostatic pressure (Smith et al. 1996). The increased aggrecan content associated with hydrostatic pressure can increase H_A and greatly reduce k while the type II collagen fibrils provide a slight increase in E . The increase in E from an up regulation of type II collagen, however, is much less than that associated with an increase in the types of collagen that exist in other soft skeletal tissues, e.g., type I collagen in fibrous tissue and fibrocartilage. This is due to the small size of type II collagen fibrils, their apparent inability to form fibers, and their more random orientation (Roth and Mow 1980).

In this study, we propose relationships linking changes in the material properties of multipotent mesenchymal tissue to mechanical loading based on the concepts described above. In this approach, fluid pressure and tensile strain regulate changes in k , H_A , and E in differentiating tissue through their effects on proteoglycan synthesis and collagen fibrillogenesis, assembly, alignment and cross-linking. We perform our simulations using an isotropic simplification with k representing the permeability in the least permeable direction (perpendicular to the fibers) and E representing the tensile elastic modulus in the stiffest direction (parallel to the fibers). H_A is equal in all directions. The input tensile and fluid stresses, initial constitutive properties of the regenerating tissue, and parameters describing the differentiation are determined from various experimental data obtained from the literature. The results of our simulations are compared to other investigators' experimental results for E , H_A , and k of cartilage, fibrocartilage, and fibrous tissue.

2

Methods

We begin with a general description of our algorithm followed by specific explanations for each of its components. After providing these explanations, we describe the parameter values used in our simulations.

In this time-dependent algorithm, we predict and track changes in E , H_A , and k of idealized mesenchymal tissue exposed to mechanical loading (Table 1, Fig. 2). We begin by specifying an initial tensile elastic modulus ($E_{mes}=E_c$ at time $t=0$), aggregate modulus ($H_{A,mes}=H_A$ at time $t=0$), and permeability ($k_{mes}=k_p$ at time $t=0$) for mesenchymal tissue. For a time step Δt , we specify the daily levels of cyclic tensile stress (σ) and fluid pressure (p) experienced by the differentiating tissue as a result of mechanical loading.

Input values of σ are used to calculate daily tensile strains. Daily tensile strains provide the stimulus for changes in E . Mikic and Carter previously defined a daily strain stimulus (Mikic and Carter 1995):

$$\zeta = \left[\sum_{\text{day}} n_i \Delta \bar{\epsilon}_i^m \right]^{1/m} \Big|_{\text{per day}} \quad (1)$$

where n_i is the number of load cycles of type i , $\bar{\epsilon}_i$ is the cyclic strain range of the energy equivalent strain for load type i , and m is an empirical constant. We may simplify this expression by assuming that this stimulus is dominated by a single load case representing a nominal peak cyclic daily strain (Wren et al. 1998). We further assume that the strain magnitude affects the stimulus to a much greater degree than the number of load cycles, i.e., m is large (Wren et al. 1998). The daily strain stimulus thus reduces to

$$\zeta \approx \Delta \bar{\epsilon} \Big|_{\text{per day}} = \epsilon \Big|_{\text{per day}} \quad (2)$$

assuming that the minimum cyclic tensile strain is zero. Peak cyclic daily strain ϵ is therefore used in place of ζ in subsequent discussion of the algorithm. As a first approximation, we assume linear elastic tensile constitutive behavior to calculate ϵ as a function of σ and E :

$$\epsilon = \sigma/E. \quad (3)$$

This strain determines the rate of modulus change \dot{E}_ϵ caused by tensile strain (Fig. 3a), occurring as a result of increased collagen fiber size, density, alignment, and cross-linking (Wren et al. 1998). The fiber-dependent rate of modulus change is then used to update the strain-dependent component of the tensile modulus:

$$E_\epsilon(t + \Delta t) = E_\epsilon(t) - \dot{E}_\epsilon \Delta t \quad (4)$$

The applied fluid pressure further modifies the tensile elastic modulus. Increased fluid pressure increases type II collagen synthesis leading to a slight increase in E via the pressure-dependent component of the tensile modulus associated with collagen fiber content, E_f (Fig. 3b). Pressure also increases proteoglycan synthesis, causing a corresponding increase to the aggregate modulus, H_A (Fig. 3c). We combine these effects to determine the pressure-dependent component of the tensile elastic modulus:

$$E_p = E_f + H_A \quad (5)$$

then calculate the total tensile modulus, E , at each time step by including both the tensile strain (Eq. 4) and fluid pressure (Eq. 5) components:

$$E = E_\epsilon + E_p \quad (6)$$

The fluid pressure stimulus further determines the proteoglycan-dependent rate of permeability change \dot{k}_p (Fig. 4) used to update the pressure-dependent component of the permeability k_p at each time step

$$k_p(t + \Delta t) = k_p(t) + \dot{k}_p \Delta t \quad (7)$$

Once we have determined the permeability component that depends on fluid pressure, we account for the effect of flow path length (Fig. 5a) using a weighting factor, q_E (Fig. 5b). We then calculate the total permeability

$$k = k_p q_E \quad (8)$$

The values of E , H_A , and k are always limited to values between specified upper and lower bounds. These bounds are phenomenological limits derived from other investigators' experimental findings for E , H_A , and k of various soft skeletal tissues (Table 2).

Once H_A , E and k are updated, we proceed to the next time step. An explanation of the stress inputs and a characterization of the relationships defining the effects of those stresses on material property adaptations of the differentiating tissue will complete our description of the algorithm.

2.1

Mechanobiological relationships and parameter values

This section describes how the mechanobiological curves (Figs. 3, 4, and 5b) were created to describe adaptation of E , H_A , and k in response to changes in tensile strain (ϵ) and fluid

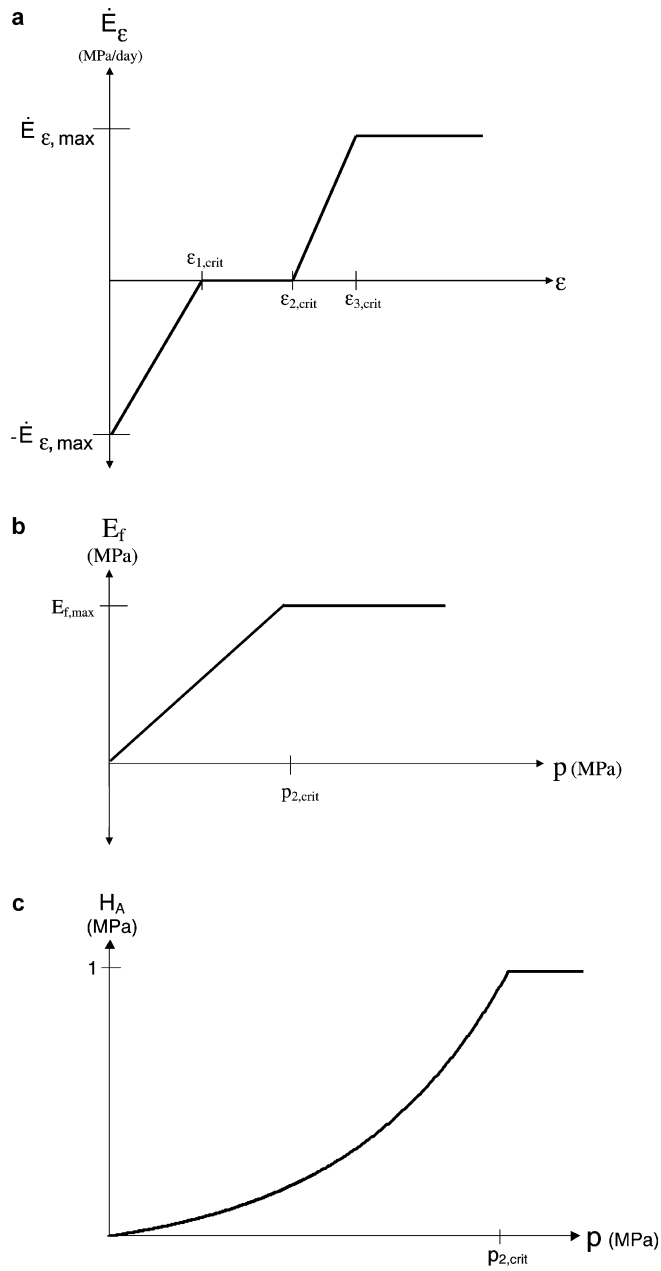


Fig. 3. Mechanobiological components of: **a** the rate of tensile elastic modulus change caused by tensile strain; **b** tensile elastic modulus change caused by fluid pressure; **c** aggregate modulus change caused by fluid pressure. $\dot{E}_{\epsilon, \max}=5.0$ MPa/day, $\epsilon_{1, \text{crit}}=0.015$, $\epsilon_{2, \text{crit}}=0.03$, $\epsilon_{3, \text{crit}}=0.04$, $E_{f, \max}=5$ MPa, and $p_{2, \text{crit}}=2.5$ MPa (Table 2)

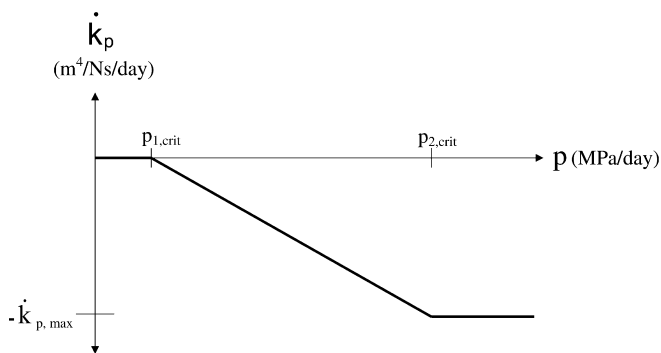


Fig. 4. Mechanobiological components of the rate of permeability change caused by fluid pressure. $p_{1, \text{crit}}=0.013$ MPa, $p_{2, \text{crit}}=2.5$ MPa, and $\dot{k}_{p, \max}=1.5 \times 10^{-15} \text{m}^4/\text{Ns}/\text{day}_{\max}$ (Table 2)

pressure (p). Parameter values were determined from experimental data in the literature (Table 2). The data come from various fibrous, cartilaginous, and fibrocartilaginous tissues from several species.

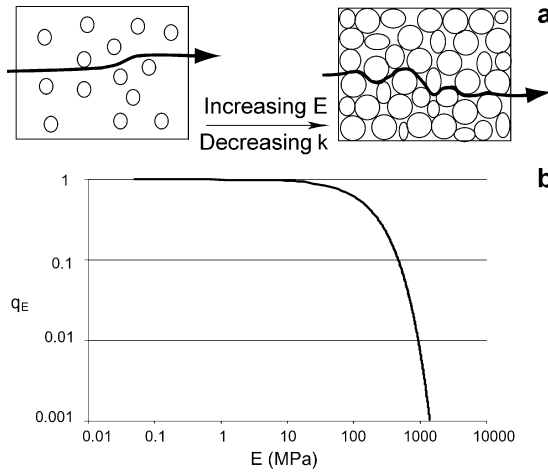


Fig. 5. a Idealized representation of increased collagen fiber size and density causing an increase in flow path length; **b** calculation of q_E , a dimensionless parameter multiplied by k_p in order to incorporate the effect of flow path length on permeability perpendicular to collagen fiber orientation (Eq. 8)

Table 2. Parameter values used in the simulations

Parameter	Value	Relevant figure/equation	Reference(s) used for value calculations
E_{mes} ($=E_e, min$)	0.05 MPa	Fig. 2	(1)
$H_{A, mes}$ ($=H_A, min$)	0.0 MPa	Fig. 2	n/a
k_{mes} ($=k_{max}$)	$1 \times 10^{-13} m^4/Ns$	Fig. 2	(2)
$\dot{E}_{e, max}$	5.0 MPa/day	Fig. 3a/Eq. 4	(3)
$\epsilon_{1, crit}$	0.015	Fig. 3a	(3), (4)
$\epsilon_{2, crit}$	0.03	Fig. 3a	(3), (4), (5)
$\epsilon_{3, crit}$	0.04	Fig. 3a	(3)
E_f, max	5 MPa	Fig. 3b	(4)
E_e, max	1500 MPa	Figs. 2, 5b/Eq. 3	(3), (6)
H_A, max	1 MPa	Fig. 3c	(7)
$\dot{k}_{p, max}$	$1.5 \times 10^{-15} m^4/Ns/day$	Fig. 4/Eqs. 7 and 9	(8)
$p_{1, crit}$	0.013 MPa	Fig. 4	(9), (10)
$p_{2, crit}$	2.5 MPa	Figs. 3b, c, 4	(11)
$k_{p, min}$	$5 \times 10^{-15} m^4/Ns$	Figs. 2, 4	(12), (13)
k_{min}	$5 \times 10^{-18} m^4/Ns$	Figs. 2, 4, 5	(3), (6), (12), (13), (14)
q_E	$e^{-0.0049 \times E}$	Fig. 5b/Eq. 8	(14)

(1) Perren and Cordey (1980); (2) Haridas et al. (1998); (3) Wren et al. (1998); (4) Akizuki et al. (1986); (5) Spilker et al. (1992); (6) Derwin et al. (1994); (7) Ateshian et al. (1994); (8) Kember and Sissons (1976); (9) Klein-Nulend et al. (1987); (10) Evanko and Vogel (1990); (11) Hodge et al. (1989); (12) Lai and Mow (1980); (13) Mansour and Mow (1976); (14) Weiss et al. (2000); n/a=not applicable

2.1.1

Rate of change of E caused by ϵ

The curve in Fig. 3a is based on work previously performed by Wren et al. (1998) to describe loading-dependent adaptations in the tensile elastic moduli of tendons and ligaments. Tensile strain stimulus values between 1.5% and 3% ($\epsilon_{1, crit}$ and $\epsilon_{2, crit}$) provide for tissue homeostasis. Physiologic tendon and ligament (Beynon et al. 1992; Wren et al. 1998), articular cartilage (Akizuki et al. 1986), and fibrocartilage (Spilker et al. 1992) tensile strains are within this range. Strains above this magnitude cause an increase in \dot{E}_e , and strains below cause a decrease in \dot{E}_e . The more extreme the tensile strains, the quicker the modulus changes with maximum rates of change $\pm \dot{E}_{e, max}$. The critical strain values ($\epsilon_{1, crit}$, $\epsilon_{2, crit}$, and $\epsilon_{3, crit}$) and the maximum rates of modulus increase and decrease ($\dot{E}_{e, max} - \dot{E}_{e, max}$) equal the values used by Wren et al. (1998). These values are based upon other investigators' experimental findings of how quickly collagen fibers can form, assemble, align, and cross-link.

2.1.2

Changes in E and H_A as a function of p

In determining the total change in tensile modulus, we also include a fluid pressure component (Fig. 3b and c, Eq. 5). It has been experimentally shown *in vitro* that intermittent fluid pressure causes chondrocytes to synthesize type II collagen (Smith et al. 1996). Assuming a similar effect during tissue differentiation, we account for an increase in E associated with an increase in type II collagen fibrogenesis stimulated by fluid pressure (E_f , Fig. 3b). Type II collagen is most prevalent in articular

cartilage, which has a tensile modulus of 5–50 MPa (Akizuki et al. 1986). The tensile modulus of articular cartilage varies as a function of its depth. The superficial zone is exposed to the highest tensile strains and has the highest tensile modulus. The middle and deep zones, however, are exposed predominantly to fluid pressure with very little tensile strain and have the lowest tensile modulus. Therefore, to account for the effects of fluid pressure alone on type II collagen fibrillogenesis, we chose a value for $E_{f,max}$ of 5 MPa for fluid pressures equal to or greater than 2.5 MPa ($p_{2,crit}$). The threshold pressure value of 2.5 MPa represents a nominal level of peak physiologic contact pressures in articular cartilage during normal daily activities such as walking (Hodge et al. 1989).

It has been shown that intermittent fluid pressure causes chondrocytes to up-regulate proteoglycan synthesis (Smith et al. 1996). To account for the dense packing of aggregates and resulting stiffening that may occur with increased proteoglycan synthesis during tissue differentiation, we calculate the aggregate modulus as a function of fluid pressure (H_A , Fig. 3c). We chose an upper bound of 1 MPa for H_A (Fig. 3c) based on other investigators' reported results of 1 MPa for the aggregate modulus of articular cartilage (Ateshian et al. 1994; Liu et al. 1997). The aggregate modulus of mesenchymal tissue is unknown. As a first approximation, we assigned an initial value of 0 MPa for $H_{A,mes}$ (Figs. 2, 3c) based on the assumption that the proteoglycan content of mesenchymal tissue is minimal compared to articular cartilage. Because the denser packing of proteoglycans may contribute slightly to the elastic modulus, we add H_A to E_f to obtain the total pressure-dependent tensile elastic modulus component E_p .

2.1.3

Rate of change of k caused by p

Fluid pressure greatly affects the permeability of differentiating tissue through its effect on proteoglycan synthesis. Cyclic fluid pressure increases proteoglycan synthesis (Smith et al. 1996). An increase in proteoglycans causes an increase in fixed charge density and, therefore, a more hydrophilic and less permeable tissue (Mow et al. 1984). The large size and dense packing of aggregates that occurs with increasing proteoglycan content further reduces k (Mow et al. 1984). We assume tissue homeostasis with respect to proteoglycan synthesis for all fluid pressures less than 0.013 MPa ($p_{1,crit}$, Fig. 4), a threshold value below which it has been experimentally shown that proteoglycan synthesis is not up-regulated (Klein-Nulend et al. 1987). Fluid pressure stimuli above this magnitude decrease the permeability until the rate of reduction in permeability reaches its limit ($-\dot{k}_{max}$) at the threshold fluid pressure of 2.5 MPa ($p_{2,crit}$). The \dot{k}_{max} value of $1.5 \times 10^{-15} \text{m}^4/\text{Ns/day}$ was determined based on the amount of time for mesenchyme, with an initial permeability of $1.0 \times 10^{-13} \text{m}^4/\text{Ns}$, to become fully differentiated into articular cartilage, shown to have a permeability on the order of $10^{-15} \text{m}^4/\text{Ns}$ (Armstrong et al. 1984). During development, full cartilage differentiation has been shown to occur in 75 days (Kember and Sissons 1976). Given that this period includes both biological and mechanical influences on tissue differentiation, we assume 75 days is the shortest time for full cartilage differentiation and maturation to occur. Thus, for a daily rate, we calculate \dot{k}_{max} as follows:

$$\dot{k}_{max} = (1.0 \times 10^{-13} - 5.0 \times 10^{-15}) \text{m}^4/\text{Ns}/75\text{days} = 1.5 \times 10^{-15} \text{m}^4/\text{Ns/day} \quad (9)$$

2.1.4

Change in k as a function of E

Permeability may be further reduced by increased flow path length that fluid must traverse before being exuded from the tissue (Fig. 5a). Flow path length transverse to the collagen fibers increases with increased fiber size and density (Chen et al. 1998; Weiss et al. 2000). Path length also increases with increased proteoglycan aggregate size and packing (Maroudas et al. 1969). Because E also increases with increased size and packing of collagen and proteoglycans, E can be used as an indicator of flow path length. Using E as such an indicator, we incorporate the dimensionless parameter q_E to account for decreased permeability associated with increased flow path length (Fig. 5b). Fibrous tissue has been experimentally shown to have a transverse permeability on the order of $10^{-16} \text{m}^4/\text{Ns}$ (Weiss et al. 2000). Since proteoglycan content is low in fibrous tissue (Evanko and Vogel 1990; Vogel et al. 1993) minimizing the binding of fluid by negatively-charged glycosaminoglycans, the three order of magnitude drop in permeability from approximately $10^{-13} \text{m}^4/\text{Ns}$ for mesenchymal tissue to $10^{-16} \text{m}^4/\text{Ns}$ for fibrous tissue is most likely a result of the extended flow path length. Beginning with our initial values of $E_{mes} = 0.05 \text{MPa}$ and $k_{mes} = 1 \times 10^{-13} \text{m}^4/\text{Ns}$ for mesenchymal tissue, we assume an exponential decline in q_E by three orders of magnitude over a tensile modulus range of 0.05–1488 MPa. The minimum tensile modulus is that of mesenchymal tissue, and the maximum is the highest modulus reported in the literature for fibrous tissue (Derwin et al. 1994). Once q_E is calculated, we multiply it by k_p to obtain the total permeability k (Eq. 8).

2.1.5

Bounds on E_c , E_p , H_A , k_p , and k

Numerical bounds for E , H_A and k are shown in Table 2. The upper bound for tensile modulus as a function of tensile strain, $E_{c, \max}$, represents the maximum attainable modulus for fibrous tissue and the lower bound, $E_{c, \min}$, the minimum modulus associated with mesenchymal tissue, E_{mes} . The upper bound for tensile modulus as a function of fluid pressure, $E_{f, \max}$, represents the maximum modulus associated with type II collagen fibrillogenesis occurring solely as a result of fluid pressure. It does not include any stiffness from type II or other types of collagen formed in response to tensile strain. The upper bound for aggregate modulus, $H_{A, \max}$, represents the aggregate modulus associated with articular cartilage. The lower bound, $H_{A, \min}$, represents the assigned initial aggregate modulus of mesenchymal tissue, $H_{A, \text{mes}}$. The upper bound for permeability, k_{\max} , represents the assigned initial permeability of mesenchymal tissue, k_{mes} . The lower bound for permeability as a function of fluid pressure alone, $k_{p, \min}$, represents the minimum attainable permeability associated with some idealized articular cartilage exposed only to fluid pressure and not experiencing any tensile stress. The lower bound for total permeability, k_{\min} , represents the permeability of idealized, highly fibrous fibrocartilage whose material properties include $E_{c, \max}$ and $k_{p, \min}$.

2.2

Sample simulations

All simulations began with material properties of multipotent mesenchymal tissue with an initial tensile modulus ($E_{\text{mes}}=E_c$ at $t=0$) of 0.05 MPa, initial aggregate modulus ($H_{A, \text{mes}}=H_A$ at $t=0$) of 0 MPa, and initial permeability ($k_{\text{mes}}=k_p$ at $t=0$) of $1 \times 10^{-13} \text{ m}^4/\text{Ns}$ (Table 3, initial). The value for E_{mes} comes from Perren and Cordey who reported a tensile modulus of 0.05 MPa for parenchyma (Perren and Cordey 1980). The permeability and aggregate modulus of mesenchymal tissue are unknown. As a first approximation, we chose k_{mes} to be on the order of $10^{-13} \text{ m}^4/\text{Ns}$, one order of magnitude greater than the longitudinal permeability of fibrous tissue, reported to be on the order of $10^{-14} \text{ m}^4/\text{Ns}$ (Haridas et al. 1998), and $H_{A, \text{mes}}$ to be 0 MPa, representative of a tissue with negligible aggrecan and compressive stiffness. Beginning with these initial properties, we ran our simulations to equilibrium (each constant time step=40 min) with three different sets of physiologic inputs for fluid pressure, p , and tensile stress, σ , representing the conditions under which articular cartilage (AC), fibrocartilage (FC), or fibrous tissue (FT) is formed (Table 3, final input).

2.2.1

Application of input stresses

Previous investigators have determined physiologic magnitudes of hydrostatic pressure in mature cartilage (Hodge et al. 1989) and fibrocartilage (Giori et al. 1993) as well as physiologic magnitudes of tensile stress in mature cartilage (Elliott et al. 1999), fibrocartilage (Tissakht and Ahmed 1995; Proctor et al. 1989), and fibrous tissue (Yamamoto et al. 1992). The fluid pressure and tensile stress magnitudes experienced by fully developed soft tissues are not appropriate for mesenchymal tissue, however, as they would likely result in failure of the mesenchyme in an in vivo situation (Loboa et al. 2001;

Table 3. Beginning with the same initial conditions for all three tissues (initial), final tensile elastic modulus, permeability, and aggregate modulus values are calculated (final output) by applying simulated physiologic stresses for each tissue (final input) to the tissue differentiation algorithm (Fig. 2). “Final input” refers to stress inputs at completion of 90-day linear ramp input period

Parameter	Articular cartilage (AC)	Fibrocartilage (FC)	Fibrous tissue (FT)	
$k_{\text{mes}}=k_{\max}$ (m^4/Ns)	1×10^{-13}	1×10^{-13}	1×10^{-13}	Initial
$E_{\text{mes}}=E_{c, \min}$ (MPa)	0.05	0.05	0.05	
$H_{A, \text{mes}}=H_{A, \min}$ (MPa)	0	0	0	
p (MPa)	10	5	n/a	Final input
σ (MPa)	0.15	10	30	
E_c (MPa)	5	333	1,000	
H_A (MPa)	1	1	0	
E_f (MPa)	5	5	0	
E_p (MPa)	6	6	0	
E (MPa)	11	339	1,000	Final output
k_p (m^4/Ns)	5×10^{-15}	5×10^{-15}	1×10^{-13}	
q_E	0.952	0.072	0.007	
k (m^4/Ns)	4.8×10^{-15}	9.5×10^{-16}	7.5×10^{-16}	

Perren and Cordey 1980). Therefore, we simulated a ramp load where the input stresses were initially zero at time $t=0$ and linearly ramped to the values for mature tissue at 90 days. We chose this time frame by reviewing a typical course of fracture healing. During tissue differentiation associated with fracture healing, mesenchymal tissue differentiates into cartilage, fibrocartilage, fibrous tissue, or bone within 3 months (Rockwood et al. 1991). Based on this time course, we chose 90 days as the minimum length of time for the full amount of loading to occur. By this point we expected that the multipotent mesenchymal tissue would have fully differentiated into cartilage, fibrocartilage, or fibrous tissue and could support the physiologic loads associated with each respective tissue.

The magnitudes of fluid pressure for AC ($p=10$ MPa) and FC ($p=5$ MPa) represent physiologic pressures reported in the literature for articular cartilage (Hodge et al. 1989) and fibrocartilage (Giori et al. 1993). We assumed fluid pressure was negligible in fibrous tissue ($p=0$ MPa) since tendons and ligaments are predominantly exposed to tensile loading. The magnitudes of tensile stress used for AC ($\sigma=0.15$ MPa), FC ($\sigma=10$ MPa), and FT ($\sigma=30$ MPa) represent physiologic tensile stresses reported in the literature for articular cartilage (Elliott et al. 1999), fibrocartilage (Proctor et al. 1989; Tissakht and Ahmed 1995), and fibrous tissue (Yamamoto et al. 1992).

3 Results

The simulations predict the largest increases in tensile elastic modulus during differentiation of mesenchymal tissue into fibrous tissue ($E=1,000$ MPa) and the smallest with differentiation into articular cartilage ($E=11$ MPa) (Fig. 6a, Table 3, final output). Tensile elastic modulus changes during differentiation into fibrocartilage fall midway between the other two tissues with a final tensile elastic modulus of 339 MPa attained within 180 days (Fig. 6a, Table 3, final output). Looking at the effects of tensile strain and fluid pressure separately, i.e., E_e and E_p , respectively, we see a marked difference in the contributions of these two components during development of the three tissues. The tensile elastic modulus of fibrous tissue attains a final value of 1,000 MPa solely as a result of tensile strain, i.e., $E=E_e$ with $E_p=0$ (Table 3, final output). Articular cartilage development, on the other hand, includes exposure to high fluid pressure with low levels of tensile strain. This results in a final tensile elastic modulus that is comprised of almost equal values for E_e (5 MPa) and E_p (6 MPa) (Table 3, final output). Fibrocartilage experiences much greater levels of tensile strain than articular cartilage but less than fibrous tissue. Accordingly, its final E_e (333 MPa) is much higher than that of articular cartilage, but still less than pure fibrous tissue (1,000 MPa, Table 3, final output). Development of fibrocartilage also includes exposure to fluid pressure, resulting in an E_p equal to 6 MPa as was seen with articular cartilage development but not with fibrous tissue development (Table 3, final output).

Therefore, beginning with the same initial conditions, our tissue differentiation algorithm predicted a diverse range of final E values among the three tissues with tensile strain having the largest impact on the fibrous tissue and fibrocartilage moduli. The tensile elastic moduli (Fig. 6a) predicted with our simulations (Fig. 3) are consistent with tensile elastic modulus values determined experimentally by other investigators for articular cartilage (Akizuki et al. 1986), fibrocartilage (Proctor et al. 1989), and fibrous tissue (Wren et al. 1998; Yamamoto et al. 1992).

Final permeabilities exhibited a reverse trend from the tensile elastic moduli results. Articular cartilage had the highest permeability ($k=4.8\times 10^{-15}$ m⁴/Ns) and fibrous tissue the lowest ($k=7.5\times 10^{-16}$ m⁴/Ns) (Fig. 6b, Table 3, final output). A function of fluid pressure alone, we see that k_p is of equal magnitude for both articular cartilage and fibrocartilage (5×10^{-15} m⁴/Ns, lower bound attained) and is two orders of magnitude lower than k_p of fibrous tissue (1×10^{-13} m⁴/Ns). Fibrous tissue, having no exposure to fluid pressure, has a k_p equal to k_{mes} , the initial mesenchymal tissue permeability (Table 3, initial). However, the permeability of fibrous tissue experiences a large decrease because of the extended flow path length associated with greatly increased collagen fiber size, density, alignment, and cross-linking (Fig. 5, Eq. 8). As a result, q_E of fibrous tissue ($q_E=0.007$) is smaller than that of fibrocartilage ($q_E=0.072$) and much smaller than that of articular cartilage ($q_E=0.952$), resulting in a final k for fibrous tissue that is less than both of these tissues (Eq. 8, Table 3, final output). However, even though q_E for fibrous tissue is 10 times smaller than q_E for fibrocartilage and over 100 times smaller than q_E for articular cartilage, the final permeabilities of all tissues vary only by an order of magnitude as a result of the impact of fluid pressure on articular cartilage and fibrocartilage permeabilities (Table 3, final output). These final calculated values of k are consistent with permeabilities determined experimentally by other investigators for articular cartilage (Proctor et al. 1989), fibrocartilage (Proctor et al. 1989), and fibrous tissue (Weiss et al. 2000).

The aggregate modulus, a function of proteoglycan content generated by fluid pressure (Fig. 3c), exhibits no change during differentiation into fibrous tissue ($H_A=0$ MPa, Fig. 6c, Table 3, final output). Mesenchymal tissue differentiation into articular and fibrocartilage, however, include high levels

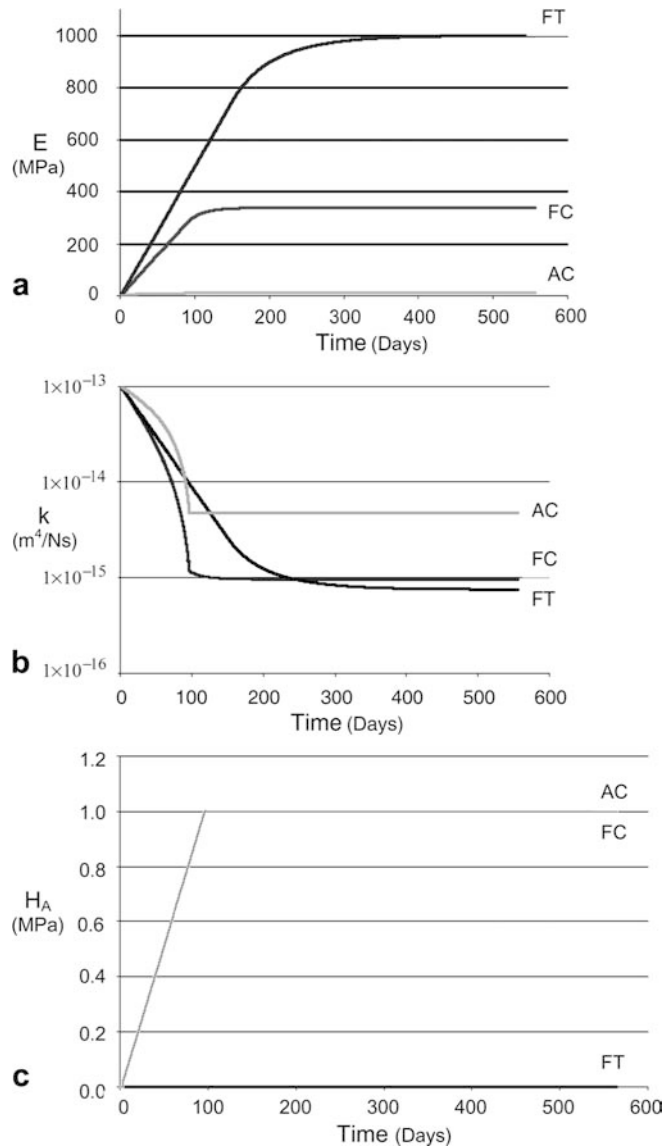


Fig. 6. Simulation results illustrating changes in: **a** tensile elastic modulus, E ; **b** permeability, k ; and, **c** aggregate modulus, H_A , during mesenchymal tissue differentiation into articular cartilage (AC), fibrocartilage (FC), or fibrous tissue (FT)

of fluid pressure so they attain the maximum aggregate modulus ($H_A=1$ MPa) within 90 days (Fig. 6c, Table 3, final output).

4 Discussion

We have presented a computational approach for simulating the effect of mechanics on material property adaptations during mesenchymal tissue differentiation. Our algorithm predicts final values of tensile elastic modulus, aggregate modulus, and permeability for articular cartilage, fibrocartilage, and fibrous tissue that are consistent with what has been observed in experimental studies.

Investigators have shown that fluid pressure increases proteoglycan and type II collagen synthesis in chondrocytes (Smith et al. 1996) and that cyclic tensile strain increases collagen fibrillogenesis by fibroblasts (Howard et al. 1998). Our tissue differentiation algorithm combines the above experimental findings with other studies looking at the effects of collagen fiber formation, assembly, alignment, and cross-linking on E (Tissakht and Ahmed 1995; Wren et al. 1998), aggrecan content on H_A (Roughley and Lee 1994) and the combination of aggrecan content (Maroudas et al. 1969) and flow path length (Chen et al. 1998; Weiss et al. 2000) on k . In doing so, our approach links mechanical loading to changes in specific tissue constituents that then lead to specific material property adaptations during mesenchymal tissue differentiation (Table 1, Fig. 2).

Since our model takes into account the primary determinants of the material properties, it can model a range of tissues. In experimental analyses of the material properties of soft skeletal tissues, researchers report a wide range of results. Various investigators attempting to empirically determine

the material properties of cartilage, for example, have obtained permeability values that vary widely depending on their experimental protocol (Athanasίου et al. 1994; Athanasίου et al. 1991; Mansour and Mow 1976; Mow et al. 1984). Given such large variety in the empirical data, it is likely that the final values of E , H_A , and k we obtain with our model will deviate from values measured in particular experimental studies. From a conceptual standpoint, however, our model is well supported. We simulate material property adaptations during mesenchymal tissue differentiation based on changes in specific tissue constituents and the effects that these changes have (Table 1). This approach allows for the application of consistent mechanobiological adaptation rules to the entire tissue differentiation process. With this approach, we can predict the formation of cartilage, fibrocartilage, and fibrous tissue, and each tissue's corresponding material properties, strictly on the basis of the mechanical environment to which the differentiating tissue is exposed.

Given that the material properties of mesenchymal tissue are still essentially unknown, the initial model we have proposed here is simplified in that we have modeled the differentiating tissue as a homogeneous, isotropic material. As more experimental data on the material properties of mesenchymal tissue become available, a more complicated material model could be introduced. We have also, as a first approximation, modeled the changes in tensile modulus assuming a linear elastic constitutive relationship. Later models could implement a nonlinear constitutive rule to calculate changes in E in order to more accurately represent the viscoelastic behavior of some soft skeletal tissues.

Results from the sample simulations provide a proof of concept for the tissue differentiation algorithm that we are presenting here for the first time. Future work could include a more elaborate computational approach with the inclusion of an initial-boundary value problem to further test this new mechanobiological concept. A finite element model of differentiating tissue exposed to external loads could be created with the differentiation algorithm applied at each node and results obtained for each time step. The values of E , H_A , and k obtained at each time step would then be used to update the material properties of the differentiating tissue at each node. Potential issues with an initial-boundary value problem would be the implementation of this algorithm in a three-dimensional context given that E is calculated in the direction of highest stiffness (parallel to the fibers) and k is calculated in the direction of least permeability (perpendicular to the fibers). Transversely isotropic material properties could be obtained, however, by outputting values for permeability in the longitudinal direction (equal to k_p) and permeability transverse to the fibers, i.e., the direction of lowest permeability (equal to k). Tensile modulus transverse to the fiber direction (assumed to be equal to E_p) would, of course, be much less than that in the longitudinal direction (equal to E).

The time course of material property changes during soft skeletal tissue differentiation is not well known. Our time-dependent model demonstrates the utility of computational approaches in describing mechanically induced material property adaptations during differentiation and soft skeletal tissue formation and may serve as a framework for future investigations and mechanobiological models.

References

- Akizuki, S.; Mow, V.C.; Müller, F.; Pita, J.C.; Howell, D.S.; Manicourt, D.H.: Tensile properties of human knee joint cartilage: I. Influence of ionic conditions, weight bearing, and fibrillation on the tensile modulus. *J Orthop Res* 4 (1986) 379–392
- Armstrong, C.G.; Lai, W.M.; Mow, V.C.: An analysis of the unconfined compression of articular cartilage. *J Biomech Eng* 106 (1984) 165–173
- Ateshian, G.A.; Lai, W.M.; Zhu, W.B.; Mow, V.C.: An asymptotic solution for the contact of two biphasic cartilage layers. *J Biomech* 27 (1994) 1347–1360
- Ateshian, G.A.; Warden, W.H.; Kim, J.J.; Grelsamer, R.P.; Mow, V.C.: Finite deformation biphasic material properties of bovine articular cartilage from confined compression experiments. *J Biomech* 30 (1997) 1157–1164
- Athanasίου, K.A.; Agarwal, A.; Dzida, F.J.: Comparative study of the intrinsic mechanical properties of the human acetabular and femoral head cartilage. *J Orthop Res* 12 (1994) 340–349
- Athanasίου, K.A.; Rosenwasser, M.P.; Buckwalter, J.A.; Malinin, T.I.; Mow, V.C.: Interspecies comparisons of in situ intrinsic mechanical properties of distal femoral cartilage. *J Orthop Res* 9 (1991) 330–340
- Atkinson, T.S.; Haut, R.C.; Altiero, N.J.: A poroelastic model that predicts some phenomenological responses of ligaments and tendons. *J Biomech Eng* 119 (1997) 400–405
- Beynon, B.; Howe, J.G.; Pope, M.H.; Johnson, R.J.; Fleming, B.C.: The measurement of anterior cruciate ligament strain in vivo. *Int Orthop* 16 (1992) 1–12
- Biot, M.: General theory of three-dimensional consolidation. *J Appl Phys* 12 (1941) 155–164
- Biot, M.: Theory of elasticity and consolidation for a porous anisotropic solid. *J Appl Phys* 26 (1955) 182–185

- Brown, T.D.; Singerman, R.J.:** Experimental determination of the linear biphasic constitutive coefficients of human fetal proximal femoral chondroepiphysis. *J Biomech* 19 (1986) 597–605
- Carter, D.R.; Beaupré, G.S.:** Skeletal tissue regeneration. In: *Skeletal function and form: mechanobiology of skeletal development, aging and regeneration*. Cambridge University Press, Cambridge (2001)
- Carter, D.R.; Beaupré, G.S.; Giori, N.J.; Helms, J.A.:** Mechanobiology of skeletal regeneration. *Clin Orthop Relat Res* 331(355 Suppl) (1998) S41–S55
- Carter, D.R.; Giori, N.:** Effect of mechanical stress on tissue differentiation in the bony implant bed. In: Davies J (ed) *The bone–biomaterial interface*. University of Toronto Press, Toronto, pp (1991) 367–379
- Carter, D.R.; Lobo Polefka, E.G.; Beaupré, G.S.:** Mechanical influences on skeletal regeneration. In: *Human biomechanics and injury prevention*. Springer-Verlag, Berlin Heidelberg New York, pp (2000) 129–136
- Chen, C.T.; Malkus, D.S.; Vanderby, R. Jr.:** A fiber matrix model for interstitial fluid flow and permeability in ligaments and tendons. *Biorheology* 35 (1998) 103–118
- Claes, L.E.; Heigele, C.A.:** Magnitudes of local stress and strain along bony surfaces predict the course and type of fracture healing. *J Biomech* 32 (1999) 255–266
- Derwin, K.A.; Soslowky, L.J.; Green, W.D.; Elder, S.H.:** A new optical system for the determination of deformations and strains: calibration characteristics and experimental results. *J Biomech* 27 (1994) 1277–1285
- Elliott, D.M.; Guilak, F.; Vail, T.P.; Wang, J.Y.; Setton, L.A.:** Tensile properties of articular cartilage are altered by meniscectomy in a canine model of osteoarthritis. *J Orthop Res* 17 (1999) 503–508
- Evanko, S.P.; Vogel, K.G.:** Ultrastructure and proteoglycan composition in the developing fibrocartilaginous region of bovine tendon. *Matrix* 10 (1990) 420–436
- Giori, N.J.; Beaupré, G.S.; Carter, D.R.:** Cellular shape and pressure may mediate mechanical control of tissue composition in tendons. *J Orthop Res* 11 (1993) 581–591
- Giori, N.J.; Ryd, L.; Carter, D.R.:** Mechanical influences on tissue differentiation at bone-cement interfaces. *J Arthrop* 10 (1995) 514–522
- Gu, W.Y.; Mao, X.G.; Foster, R.J.; Weidenbaum, M.; Mow, V.C.; Rawlins, B.A.:** The anisotropic hydraulic permeability of human lumbar annulus fibrosus. Influence of age, degeneration, direction, and water content. *Spine* 24 (1999) 2449–2455
- Haridas, B.; Butler, D.; Malaviya, P.; Awad, H.; Boivin, G.; Smith, F.:** In vivo stresses correlate with cellular morphology in the fibrocartilage-rich region of the rabbit flexor tendon. In: *Proceedings of the 44th Annual Meeting, Orthopaedic Research Society, New Orleans, La.* (1998)
- Higginson, G.R.; Snaith, J.E.:** The mechanical stiffness of articular cartilage in confined oscillating compression. *Eng Med* 8 (1979) 11–14
- Hodge, W.A.; Carlson, K.L.; Fijan, R.S.; Burgess, R.G.; Riley, P.O.; Harris, W.H.; Mann, R.W.:** Contact pressures from an instrumented hip endoprosthesis. *J Bone Joint Surg Am* 71 (1989) 1378–1386
- Howard, P.S.; Kucich, U.; Taliwal, R.; Korostoff, J.M.:** Mechanical forces alter extracellular matrix synthesis by human periodontal ligament fibroblasts. *J Periodont Res* 33 (1998) 500–508
- Huiskes, R.; van Driel, W.; Prendergast, P.; Soballe, K.:** A biomechanical regulatory model for periprosthetic fibrous-tissue differentiation. *J Mater Sci Mater Med* 8 (1997) 785–788
- Ilizarov, G.A.:** The tension–stress effect on the genesis and growth of tissues. Part I. The influence of stability of fixation and soft-tissue preservation. *Clin Orthop* 238 (1989) 249–281
- Joshi, M.D.; Suh, J.K.; Marui, T.; Woo, S.L.:** Interspecies variation of compressive biomechanical properties of the meniscus. *J Biomed Mater Res* 29 (1995) 823–828
- Jurvelin, J.S.; Buschmann, M.D.; Hunziker, E.B.:** Optical and mechanical determination of Poisson’s ratio of adult bovine humeral articular cartilage. *J Biomech* 30 (1997) 235–241
- Kember, N.F.; Sissons, H.A.:** Quantitative histology of the human growth plate. *J Bone Joint Surg Br* 58 (1976) 426–435
- Klein-Nulend, J.; Veldhuijzen, J.P.; van de Stadt, R.J.; van Kampen, G.P.; Kuijjer, R.; Burger, E.H.:** Influence of intermittent compressive force on proteoglycan content in calcifying growth plate cartilage in vitro. *J Biol Chem* 262 (1987) 15490–15495
- Lai, W.; Mow, V.:** Drag-induced compression of articular cartilage during a permeation experiment. *Biorheology* 17 (1980) 111–123
- Levenston, M.; Frank, E.; Grodzinsky, A.:** Variationally derived 3-field finite element formulations for quasistatic poroelastic analysis of hydrated biological tissues. *Comput Meth Appl Mech Eng* 156 (1998) 231–246
- Li, L.P.; Buschmann, M.D.; Shirazi-Adl, A.:** A fibril reinforced nonhomogeneous poroelastic model for articular cartilage: inhomogeneous response in unconfined compression. *J Biomech* 33 (2000) 1533–1541
- Li, L.P.; Soulhat, J.; Buschmann, M.D.; Shirazi-Adl, A.:** Nonlinear analysis of cartilage in unconfined ramp compression using a fibril reinforced poroelastic model. *Clin Biomech* 14 (1999) 673–682
- Liu, G.T.; Lavery, L.A.; Schenck, R.C. Jr.; Lanctot, D.R.; Zhu, C.F.; Athanasiou, K.A.:** Human articular cartilage biomechanics of the second metatarsal intermediate cuneiform joint. *J Foot Ankle Surg* 36 (1997) 367–374
- Lobo, E.; Beaupré, G.; Carter, D.:** Mechanobiology of initial pseudarthrosis formation with oblique fractures. *J Orthop Res* 19 (2001) 1067–1072
- Mansour, J.M.; Mow, V.C.:** The permeability of articular cartilage under compressive strain and at high pressures. *J Bone Joint Surg Am* 58 (1976) 509–516
- Maroudas, A.; Muir, H.; Wingham, J.:** The correlation of fixed negative charge with glycosaminoglycan content of human articular cartilage. *Biochim Biophys Acta* 177 (1969) 492–500
- Meroi, E.A.; Natali, A.N.:** A numerical approach to the biomechanical analysis of bone fracture healing. *J Biomed Eng* 11 (1989) 390–397
- Mikic, B.; Carter, D.R.:** Bone strain gage data and theoretical models of functional adaptation. *J Biomech* 28 (1995) 465–469

- Mow, V.C.; Gibbs, M.C.; Lai, W.M.; Zhu, W.B.; Athanasiou, K.A.: Biphasic indentation of articular cartilage-II. A numerical algorithm and an experimental study. *J Biomech* 22 (1989) 853-861
- Mow, V.C.; Holmes, M.H.; Lai, W.M.: Fluid transport and mechanical properties of articular cartilage: a review. *J Biomech* 17 (1984) 377-394
- Mow, V.C.; Kuei, S.C.; Lai, W.M.; Armstrong, C.G.: Biphasic creep and stress relaxation of articular cartilage in compression? Theory and experiments. *J Biomech Eng* 102 (1980) 73-84
- Mow, V.C.; Zhu, W.; Ratcliffe, A.: Structure and function of articular cartilage and meniscus. In: Mow VC, Hayes WC (eds) *Basic orthopaedic biomechanics*. Raven Press, New York, pp (1991) 143-198
- Pauwels, F.: *Biomechanics of the locomotor apparatus : contributions on the functional anatomy of the locomotor apparatus*. Springer-Verlag, Berlin Heidelberg New York (1980)
- Perren, S.; Cordey, J.: The concept of interfragmentary strain. In: Uthoff HK (ed) *Current concepts of internal fixation of fractures*. Springer-Verlag, New York Berlin Heidelberg, pp (1980) 63-77
- Prendergast, P.J.; Huijkes, R.; Soballe, K.: ESB Research Award 1996. Biophysical stimuli on cells during tissue differentiation at implant interfaces. *J Biomech* 30 (1997) 539-548
- Proctor, C.S.; Schmidt, M.B.; Whipple, R.R.; Kelly, M.A.; Mow, V.C.: Material properties of the normal medial bovine meniscus. *J Orthop Res* 7 (1989) 771-782
- Rockwood, C.A.; Green, D.P.; Bucholz, R.W.: *Rockwood and Green's fractures in adults*. Lippincott, Philadelphia, Pa (1991)
- Roth, V.; Mow, V.C.: The intrinsic tensile behavior of the matrix of bovine articular cartilage and its variation with age. *J Bone Joint Surg Am* 62 (1980) 1102-1117
- Roughley, P.J.; Lee, E.R.: Cartilage proteoglycans: structure and potential functions. *Microsc Res Technol* 28 (1994) 385-397
- Smith, R.L.; Rusk, S.F.; Ellison, B.E.; Wessells, P.; Tsuchiya, K.; Carter, D.R.; Caler, W.E.; Sandell, L.J.; Schurman, D.J.: In vitro stimulation of articular chondrocyte mRNA and extracellular matrix synthesis by hydrostatic pressure. *J Orthop Res* 14 (1996) 53-60
- Soltz, M.A.; Ateshian, G.A.: Experimental verification and theoretical prediction of cartilage interstitial fluid pressurization at an impermeable contact interface in confined compression. *J Biomech* 31 (1998) 927-934
- Soltz, M.A.; Ateshian, G.A.: Interstitial fluid pressurization during confined compression cyclical loading of articular cartilage. *Ann Biomed Eng* 28 (2000) 150-159
- Soulhat, J.; Buschmann, M.D.; Shirazi-Adl, A.: A fibril-network-reinforced biphasic model of cartilage in unconfined compression. *J Biomech Eng* 121 (1999) 340-347
- Spilker, R.L.; Donzelli, P.S.; Mow, V.C.: A transversely isotropic biphasic finite element model of the meniscus. *J Biomech* 25 (1992) 1027-1045
- Tissakht, M.; Ahmed, A.M.: Tensile stress-strain characteristics of the human meniscal material. *J Biomech* 28 (1995) 411-422
- Vogel, K.G.; Ordög, A.; Pogány, G.; Oláh, J.: Proteoglycans in the compressed region of human tibialis posterior tendon and in ligaments. *J Orthop Res* 11 (1993) 68-77
- Weiss, J.; Maakestad, B.; Nisbet, J.: The permeability of human medial collateral ligament. In: *Proceedings of the 46th Annual Meeting, Orthopaedic Research Society, Orlando, FL (2000)*
- Wren, T.A.; Beaupré, G.S.; Carter, D.R.: A model for loading-dependent growth, development, and adaptation of tendons and ligaments. *J Biomech* 31 (1998) 107-114
- Wren, T.A.; Beaupré, G.S.; Carter, D.R.: Mechanobiology of tendon adaptation to compressive loading through fibrocartilaginous metaplasia. *J Rehabil Res Dev* 37 (2000) 135-143
- Wren, T.A.; Carter, D.R.: A microstructural model for the tensile constitutive and failure behavior of soft skeletal connective tissues. *J Biomech Eng* 120 (1998) 55-61
- Yamamoto, N.; Hayashi, K.; Kuriyama, H.; Ohno, K.; Yasuda, K.; Kaneda, K.: Mechanical properties of the rabbit patellar tendon. *J Biomech Eng* 114 (1992) 332-337